Vortical structure in a forced plane mixing layer

By R. L. LeBoeuf

The objective of this phase of an ongoing study is to obtain detailed three-dimensional phase-averaged measurements of forced mixing layer vorticity development and evolution. Acoustic forcing is being used to phase-lock the initial development and subsequent pairing of the spanwise vortical structures. Phase-averaged measurements of the three velocity components will permit the study of three-dimensional vorticity distributions without invoking Taylor's hypothesis which is known to introduce uncertainty. Currently two sine waves, one at the fundamental roll-up frequency and the second, its subharmonic, are being used to force the initial roll-up and first pairing of the spanwise rollers. The two-dimensional measurements described in this report were obtained in order to determine the best operating conditions for the detailed three-dimensional study of the mixing layer undergoing pairing via various pairing mechanisms.

1. Motivation and objectives

Being one of the fundamental transitional flows as well as a technologically significant flow, the mixing layer has been scrutinized for many decades. Among the experimental investigations, many, especially the earlier studies, involved one- and two-dimensional measurements of time-averaged turbulence quantities. The results of these studies have been useful for corroborating turbulence theories and tuning turbulence models. In the late sixties and early seventies, the advent of the search for coherent structures and their dynamics lead to more detailed studies of mixing layer structure. For example, Winant & Browand (1974) showed that spanwise vortex pairing is a controlling factor for mixing layer growth. Coherent structure eduction, aided by artificial excitation of the mixing layer roll-up and pairing, has continued through to the present.

In addition to the two-dimensional coherent structures discussed above, signs of spatially coherent streamwise structures in plane mixing layers were identified in flow visualization studies at Caltech during the early eighties (eg. Breidenthal 1981 and Bernal & Roshko 1986). Models of the three-dimensional mixing layer structure (eg. Bernal 1981) and attempts to quantify the observations quickly followed. These earlier studies were limited to three-dimensional time-averaged measurements (Bell & Mehta 1992), measurements of partial vorticity (Huang & Ho 1990 and Nygaard & Glezer 1991) and/or the extension of temporal measurements to three-dimensional grids using Taylor's hypothesis (Nygaard & Glezer 1991 and Tung 1992). The appearance of mean streamwise vorticity in time-averaged measurements confirmed the existence of coherent spatially-stationary secondary vorticity in mixing layers (Bell & Mehta 1992). However, the details and interactions of the secondary structure are lost through the averaging process. Furthermore, Taylor's hypothesis was

shown by Zaman & Hussein (1981) to be inadequate for transforming temporal measurements to a spatial grid for a circular jet – especially in regions of vortex interactions. Included in this report is an extensive comparison of data generated using Taylor's hypothesis to their true counterparts which indicates that the same deficiencies also apply to a two-stream plane mixing layer.

In addition to the large set of mixing layer measurements, there have been several computations of the mixing layer development. In one study related to the results detailed in this report, a spatial simulation employing a two-dimensional vortex method was used by Inoue (1992) to investigate the effect of double-frequency forcing on the initial spanwise vortex development and subsequent pairing. The dependence of the pairing mechanism on the relative forcing signal phase, demonstrated earlier using two-dimensional temporal simulations (eg. Riley & Metcalfe 1980), was confirmed. Three-dimensional spatial simulations of the mixing layer performed in the late eighties (Buell 1991) clearly showed the presence and development of the primary and secondary vorticity. Spatial simulations soon gave way to the more economical temporal simulations (eg. Rogers & Moser 1992, Moser & Rogers 1993). The sequence of temporal simulations which have since been conducted have been used to clarify many of the details of the three-dimensional evolution of plane mixing layers. However, limits imposed by the expense associated with computational grid size and computation time make it difficult to evaluate the relationship between the time-averages and the true structure using simulations, especially in in the mid- to far-field regions of mixing layer development.

The objective of this study is to investigate the development of three-dimensionality and transition to turbulence in a forced plane two-stream mixing layer. Acoustic forcing is being used to generate specific pairing mechanisms which would otherwise occur randomly in an unforced mixing layer. Phase-averaged measurements are being used to then quantify the resulting vorticity development and interaction. These measurements, coupled with the previous direct numerical simulation results, should shed new light on the development of spatially evolving mixing layers. In particular, the relationship between time-averaged measurements and the three-dimensional structure will be clarified.

2. Accomplishments

2.1 The experiment

The experiments were conducted in a mixing layer wind tunnel specifically designed for free-shear flow experiments (Bell & Mehta 1989). The wind tunnel consists of two separate legs which are driven independently by centrifugal blowers connected to variable speed motors. The two streams merge at the sharp trailing edge of a slowly tapering splitter plate; the included angle at the splitter plate edge, which extends 15 cm into the test section, is about 1°. The test section is 36 cm in the cross-stream direction, 91 cm in the spanwise direction, and 366 cm in length. An adjustable side-wall is used to zero the streamwise pressure gradient. To facilitate 3-D traversing, a slotted 3/32 inch thick aluminum plate was mounted on the traverse which moves the probe in the streamwise (X) direction. The plate,

which slides against the inside surface of the one side-wall, was large enough to allow traversing in the streamwise direction of approximately 30 cm for a fixed traversing table location.

In the present experiments, the two sides of the mixing layer were set to 12 m/s and 7.2 m/s for a velocity ratio equal to that used by Bell & Mehta (1992) in the same facility, $r = U_2/U_1 = 0.6$ [$\lambda = (U_1 - U_2)/(U_1 + U_2) = 0.25$]. These operating conditions resulted in the lowest initial wake unsteadiness levels and free-stream streamwise turbulence levels (u'/U_e) of approximately 0.2% and the transverse levels (v'/U_e and w'/U_e) of approximately 0.05%. The mean core-flow was found to be uniform to within 0.5% and cross-flow angles were less than 0.25°. The boundary layers on the splitter plate were laminar at these operating conditions.

Velocity measurements were made using a single cross-wire probe which is rotated in order to measure flow in two-coordinate planes. The *Dantec* cross-wire probe (Model 55P51) consisted of 5 μm platinum-plated tungsten sensing elements approximately 1 mm long with approximately 1 mm spacing. The probes were calibrated statically in the potential core of the flow assuming a 'cosine-law' response to yaw, with the effective angle determined by calibration. The analog signals generated by *DISA* (Model 55M01) anemometers were sampled using a *Tustin* (Model 110-9C) 15 bit simultaneous sample-and-hold A/D converter with a multiplexed connection to the computer.

Conversion of the hot-wire data to effective normal velocities is achieved on-line through the use of look-up tables. The linear decoding afforded by using the cosine-law allows post-experimental calculation of velocity statistics from effective velocity statistics written to disk. This scheme, used for both time averages and phase averages, substantially decreased (by approximately 60%) the experimental run-time calculations required relative to calculating velocities for each time step and subsequently averaging. Similarly, for velocity spectra measurements, the effective velocity spectra were calculated on-line using a Fast Fourier Transform (FFT) routine, output to disk, and later decoded. The increased experimental run-time calculations of this approach are more than offset by the savings in disk read/writes required by saving entire time-series for post-processing of spectra. Additional time savings were gleaned by using double-buffering, a scheme whereby a block of data is acquired via the A/D converter and a previously acquired block of data is processed *simultaneously*. In the future, a multi-tasking scheme may be employed in order to perform the calculations during both the data acquisition *and* traversing times.

Due to the large quantities of data required by this study, many aspects of this experiment were automated. The data acquisition and control systems are shown diagrammatically in Fig. 1. A *DEC Micro Vax II* computer using the VMS operating system is the platform. While taking data for a single run, typically over the course of *many days*, the MicroVax is able to coordinate the traversing, A/D control, blower speed control, and relative phase of forcing signals without human intervention. To insure measurement accuracy, a number of conditions including blower drift, hot-wire calibration drift, forcing signal variation, and traverse malfunction are tested periodically during every data acquisition run.

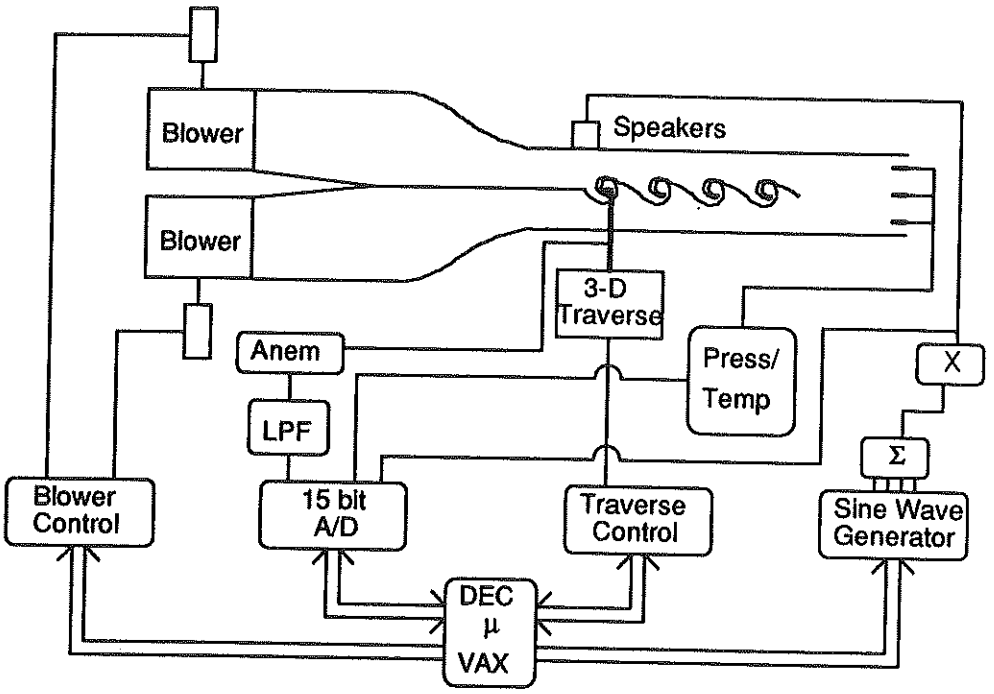

FIGURE 1. Forced mixing layer data acquisition and control system.

Since the temperature in the laboratory may change by 10-15°C over the course of a day, the test-section velocity and hot-wire calibration drift-checks are performed approximately every ten minutes. If, during a drift-check, the cross-wire measurements differ from the reference (measured using a pitot-static tube) by more than 1.5%, then a new constant angle calibration is performed and new effective velocity look-up tables are calculated. Note, since the yaw calibration is not automated, the effective wire angles obtained from a yaw calibration at the beginning of each run are maintained for an entire run. This is not expected to introduce significant error into the measurements since the wire angles would not be expected to change rapidly. If either the hot-wire drift or the test-section velocity drift exceeds 2%, the data acquired between the previous drift-check and the current one is re-acquired.

Since the traverse employs stepper motors operated in open-loop, the integrity of the traverse locations is also tested. The threshold levels of roller actuated switches are used to determine the calibration/drift-check location during each drift-check. If the traverse is found to deviate more than 5% of the grid spacing (i.e. typically 0.5% of the spanwise structure size), then the previous data is re-acquired. After each drift-check, the test-section velocities are adjusted to the set-points (12 and 7.2 m/s) to within 0.3%. The forcing signals are measured before and after each plane to verify their integrity as well. Note, the true relative forcing signal phase was determined by correlating the sine-wave generator outputs and phase-average microphone measurements of the speaker output.

A digital sine-wave generator capable of outputting up to four signals simultaneously was designed (by Dr. J. H. Watmuff) and built for this project. The amplitudes and frequencies are tunable from the front panel of the device while the relative phase of the sine-waves can be adjusted using front panel BCD switches or digital input. The digital control of the relative phase by the MicroVax was used during sequential runs for which the only parameter varied from one run to the next was the relative phase. The forcing signals used to obtain the results shown in this report consisted of the sum of a sine-wave at the fundamental roll-up frequency (obtained from centerline spectra) and its subharmonic:

$$s(t) = A_1 sin 2\pi f_1 t + A_2 sin(2\pi f_2 t + \beta_2)$$

where $f_1 = 500$ Hz and $f_2 = 250$ Hz. The amplitude ratio ($a = A_2/A_1$), which largely dictates the pairing location for multiple-frequency forcing (Inouye 1992), was set equal to 2.0 for all of the measurements described in this report. However, measurements of the speaker output indicated that the amplitude ratio was in approximately 40. This forced the first pairing to occur at about 15 cm from the splitter plate trailing edge.

The individual sine-waves were combined using a simple summing circuit and output by an audio amplifier to a spanwise array of three four inch speakers. The frequency response of the amplifier (*Realistic* SA-155) and speakers were rated at 20 Hz to 25 kHz and 55 Hz to 5 kHz, respectively. The speakers were mounted in a rectangular wood box which, with the exception of a vertical slot, was lined with foam to decrease the occurrence of acoustic reflections. The speakers were placed directly across from the splitter plate trailing edge (see Fig. 1) at a side-wall slot location. Measurements along the slot of the speaker box with a microphone showed that the pressure induced by the speakers was uniform within 3% along the span of the test-section. The sine-wave generator also output digital start sample pulses and a clock signal with 2^n pulses per cycle, where n can be any integer from 3 to 8. These signals were used to synchronize the A/D sampling with the forcing signals. For the phase-averages shown in the next section, 768 ensembles of 16 samples per phase were measured. The internal A/D clock set to 2500 Hz was used for the spectra measurements described in the next section. Low-pass filters (Krohn-Hite Model 3343, LPF in Fig. 1) set to 1200 Hz were used to avoid aliasing the hot-wire spectra measurements. Five hundred blocks were found to adequately converge the 256 sample spectral estimates.

2.2 Results and discussion

2.2.1 Spanwise structure coherence

Recognizing the importance of the structure-to-structure repeatability gained by forcing the mixing layer, the first set of measurements were used to identify the relative phase of forcing signals resulting in optimal coherence of the pairing spanwise structures. Given the triple decomposition representation of the flow component $u_i(\mathbf{x}, t)$:

$$u_i(\mathbf{x}, t) = \overline{u}_i(\mathbf{x}) + \tilde{u}_i(\mathbf{x}, t) + u_i''(\mathbf{x}, t)$$

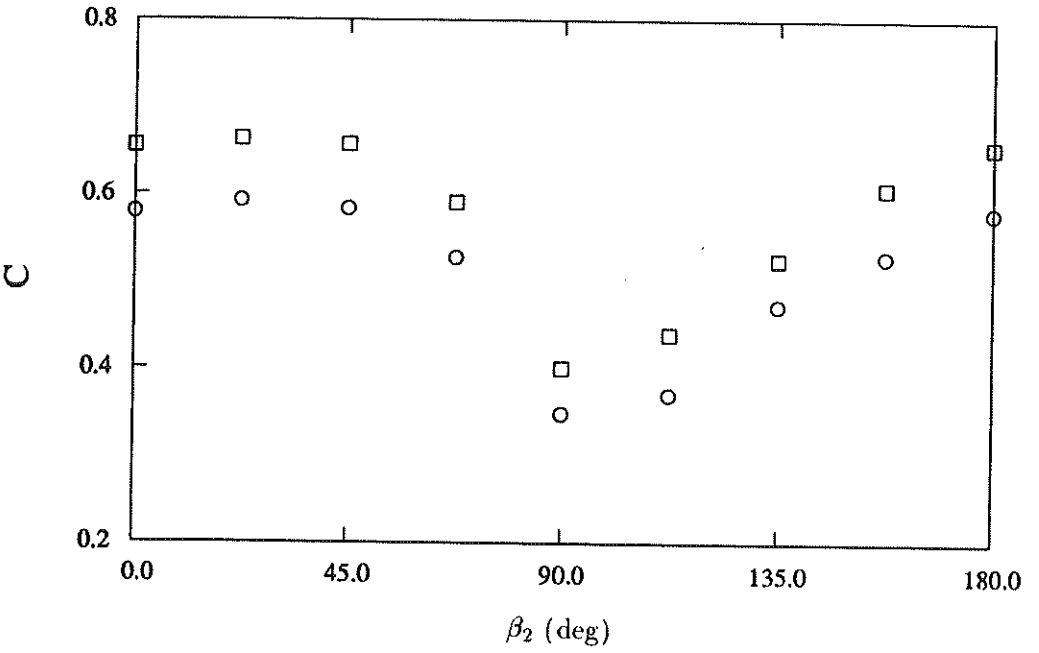

FIGURE 2. Centerplane average coherence, u o ; v □ .

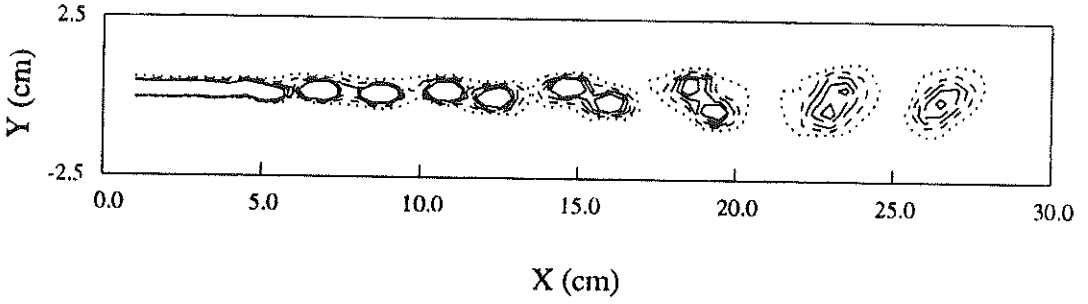

FIGURE 3. Centerplane spanwise vorticity normalized by $U_1 - U_2$ at $T = 0$ for $\beta_2 = 22.5°$, 0.125 ····· ; 0.25 - - - - ; 0.375 — — — ; 0.5 — — ; 0.625 ——— (s^{-1}).

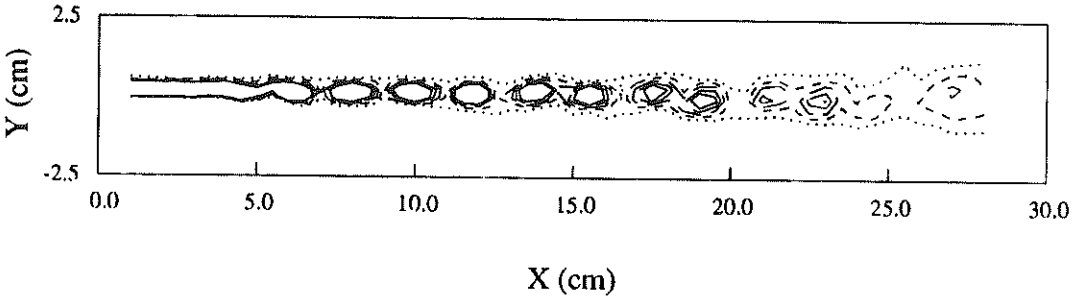

FIGURE 4. Centerplane spanwise vorticity normalized by $U_1 - U_2$ at $T = 0$ for $\beta_2 = 90°$, 0.125 ····· ; 0.25 - - - - ; 0.375 — — — ; 0.5 — — ; 0.625 ——— (s^{-1}).

where $\overline{u}_i(\mathbf{x}) = \overline{u_i(\mathbf{x},t)}$ is the local time-average, $\tilde{u}_i(\mathbf{x},t) = < u_i(\mathbf{x},t) > $ is the periodic unsteadiness, and $u_i''(\mathbf{x},t)$ is the random component of $u_i(\mathbf{x},t)$. Note, the overbar denotes time-averaging while the brackets (<>) denote a phase-locked ensemble average over one fundamental period. The measure of coherence used to characterize the relative success of forcing was the ratio of the periodic contribution to the normal Reynolds stress to the total normal Reynolds stress:

$$C_i = \frac{\overline{< u_i(\mathbf{x},t) >^2}}{\overline{(< u_i(\mathbf{x},t) > + u_i''(\mathbf{x},t))^2}}.$$

This quantity was averaged over a centerplane oriented normal to the mixing layer ($X - Y$ plane) for nine different relative phases (β_2) ranging from 0 to 180°. Note, the phase is defined such that the forcing signal repeats for every 180° shift of the subharmonic relative to the fundamental. The measurement grid consisted of 55 uniformly spaced X locations in the range 1 to 28 cm and 13 uniformly spaced Y locations distributed over a linearly increasing range of -1 to 1 cm at $X = 1$ cm to the range -2.5 to 2.5 cm at $X = 28$ cm. The resulting distribution of the coherence versus relative forcing signal phase is shown in Fig. 2. Clearly, the coherence displays a broad peak between approximately 0° and 45°, while the minimum is much sharper at a phase of 90°. The resulting centerplane phase-averaged spanwise vorticity contours for the two extreme cases each at dimensionless time $T = 0$ are shown in Figs. 3 ($\beta_2 = 22.5°$) and 4 ($\beta_2 = 90°$). Clearly, Fig. 3 illustrates the traditional pairing mechanism for which two adjacent vortices begin to corrotate and finally merge into a single larger vortex. This results in a higher coherence than the shredding mechanism illustrated in Fig. 4. Double-frequency forcing with relative phase (β_2) set equal to 22.5° was therefore chosen for measurements of the usual pairing mechanism. These results confirm that double-frequency forcing with a relative phase of 90° results in shredding/tearing as shown by Riley & Metcalfe (1980) using a 2-D temporal simulation.

To help clarify this observed variation of the mean coherence parameter, the spatial distributions of the coherence parameter for the phases corresponding to the peak mean coherence ($\beta_2 = 22.5°$ and 4 $\beta_2 = 90°$) are included in Figs. 5 and 6, respectively. The relatively higher average u component phase coherence for the optimum forcing signal phase setting results from the recovery of the coherence near the onset of pairing ($X = 15$ cm) and the minor recovery at the edges of the mixing layer after pairing [see Figs. 5 (*a*) and 6 (*a*)]. Figures 5 (*b*) and 6 (*b*) show that at the optimum phase, the v component coherence recovers to its peak value immediately after pairing. This recovery does not occur for the shredding interaction. It remains to be shown whether the loss of coherence in either of these cases is due to large-scale jitter or small-scale motions. One possible scheme for isolating the contributions of the small-scale motions and large-scale jitter is to simultaneously phase-average the raw hot-wire signals and their low-pass filtered counterparts. For appropriate low-pass filter settings, the ratio of the random contribution of the filtered signals to the Reynolds stress to the total random contribution to the Reynolds stress would be indicative of the large scale jitter contribution to the total randomness.

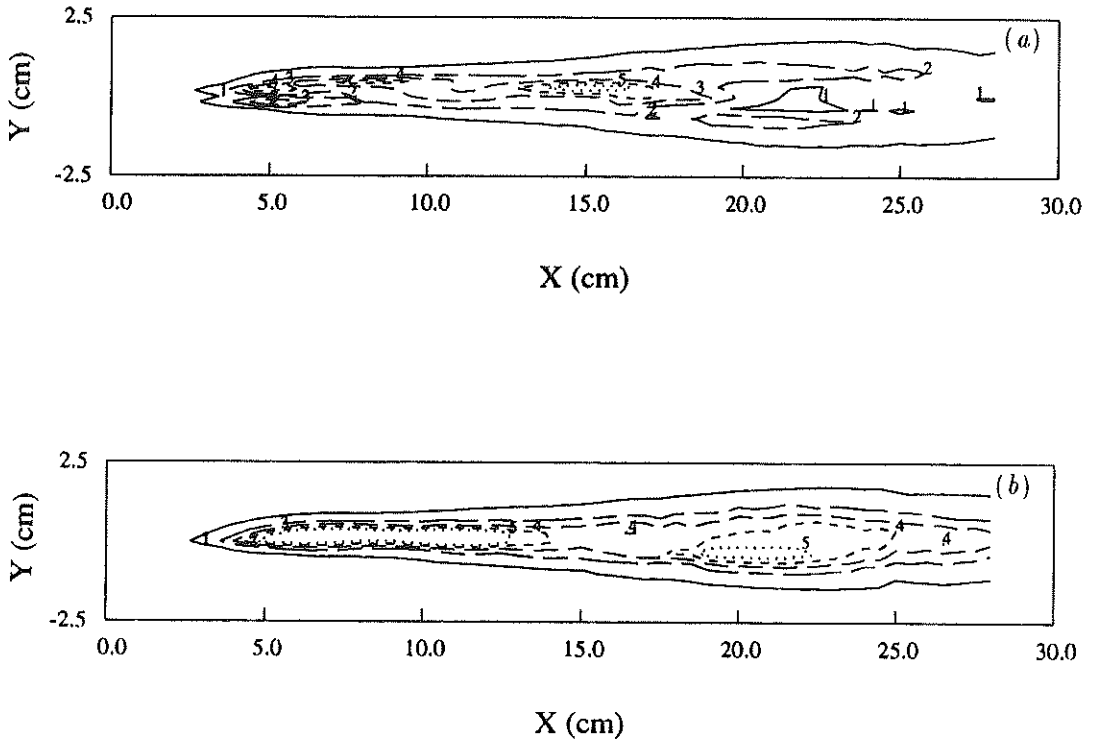

FIGURE 5. Centerplane coherence distribution for $\beta_2 = 22.5°$. *(a)* u *(b)* v; 0.05 ——— ; 0.275 — — ; 0.5 — — — ; 0.725 - - - - ; 0.95 ····· .

2.2.2 Centerline spectra

With the exception of a relative phase shift, the coherence versus relative phase relationship shown in Fig. 2 resembles the subharmonic amplification rate measured in the near field of a double-frequency forced water tunnel mixing layer by Zhang, Ho & Monkewitz (1985). The phase shift, as mentioned above, is in part due to the audio amplifier and may be augmented by the additional transfer function associated with the speakers. Nevertheless, to investigate this possible relationship further, centerline spectra of the forced mixing layer were measured for relative phases ranging from 0° to 180° in increments of 22.5°. For each phase, u and v spectra were measured for X ranging from 1 to 28 cm in 1 cm increments. Contours of the streamwise $[S_{uu}(f_1, X)]$ and transverse $[S_{vv}(f_1, X)]$ spectra at the fundamental forcing frequency (f_1) are shown in Fig. 7 (a) and (b). Similarly, the measured spectra at the subharmonic frequency (f_2) are shown in Figs. 8 (a) and (b). For the phase range between 90° and 135°, the subharmonic spectra of Figs. 8 (a) and (b) begin to rise during the onset of the initial roll-up (at approximately $X = 5$ cm) and maintain a plateau until pairing is complete. For that same range of forcing signal phases, Figs. 7 (a) and (b) show a rapid amplification of the energy at the fundamental which begins to decay as pairing progresses. For the forcing phase leading to shredding ($\beta_2 = 90°$), the subharmonic energy grows less rapidly and does not

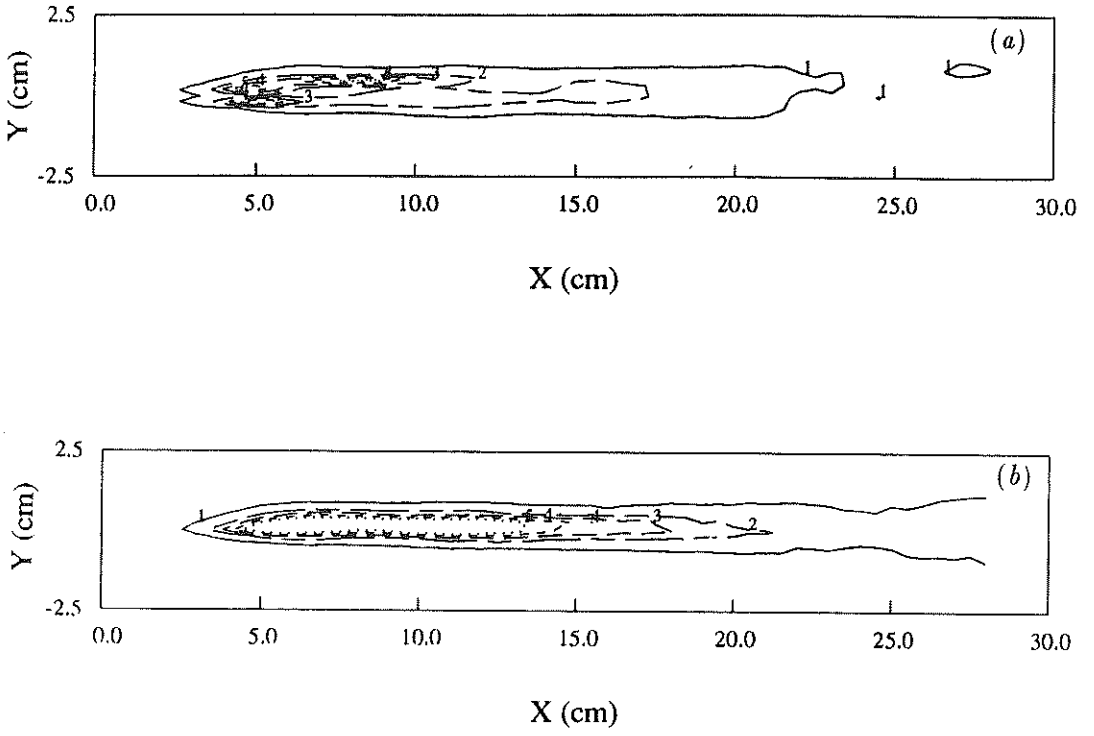

FIGURE 6. Centerplane coherence distribution for $\beta_2 = 90°$. *(a) u (b) v*; 0.05 ——— ; 0.275 — — — ; 0.5 — — — ; 0.725 - - - - ; 0.95 ····· .

reach as high an amplitude as that for the high coherence phase range. Figure 7 (*b*) illustrates the weak dependence of the initial growth of the energy at the fundamental forcing frequency on the relative forcing phase; a result demonstrated by Zhang, Ho and Monkewitz (1985). Furthermore, the spectra at the fundamental frequency decays more quickly for forcing signal phase leading to shredding. The combination of lower sustained subharmonic energy growth and more rapid fundamental energy decay are apparently responsible, or at least symptomatic, of a decrease in the coherence of the spanwise structure.

2.2.3 Taylor's hypothesis error

The sequence of centerplane phase-averaged $u - v$ data obtained with forcing relative phase set to 112.5° were also used to demonstrate the limitation of Taylor's hypothesis (herein denoted TH) for the plane mixing layer. For each streamwise location between $X = 10$ cm and $X = 28$ cm, TH was used to generate spatial distributions of streamwise (u) and transverse (v) velocity components at upstream locations using phase averaged data at different non-dimensional times. Note, a single convection velocity ($U_c = 9.6$ m/s) equal to the average of the streamwise velocities on the two sides of the layer (suggested by Zaman & Hussein 1981 based on jet mixing layer comparisons) was transformed to $\tilde{X} = X - U_c t$. The resulting

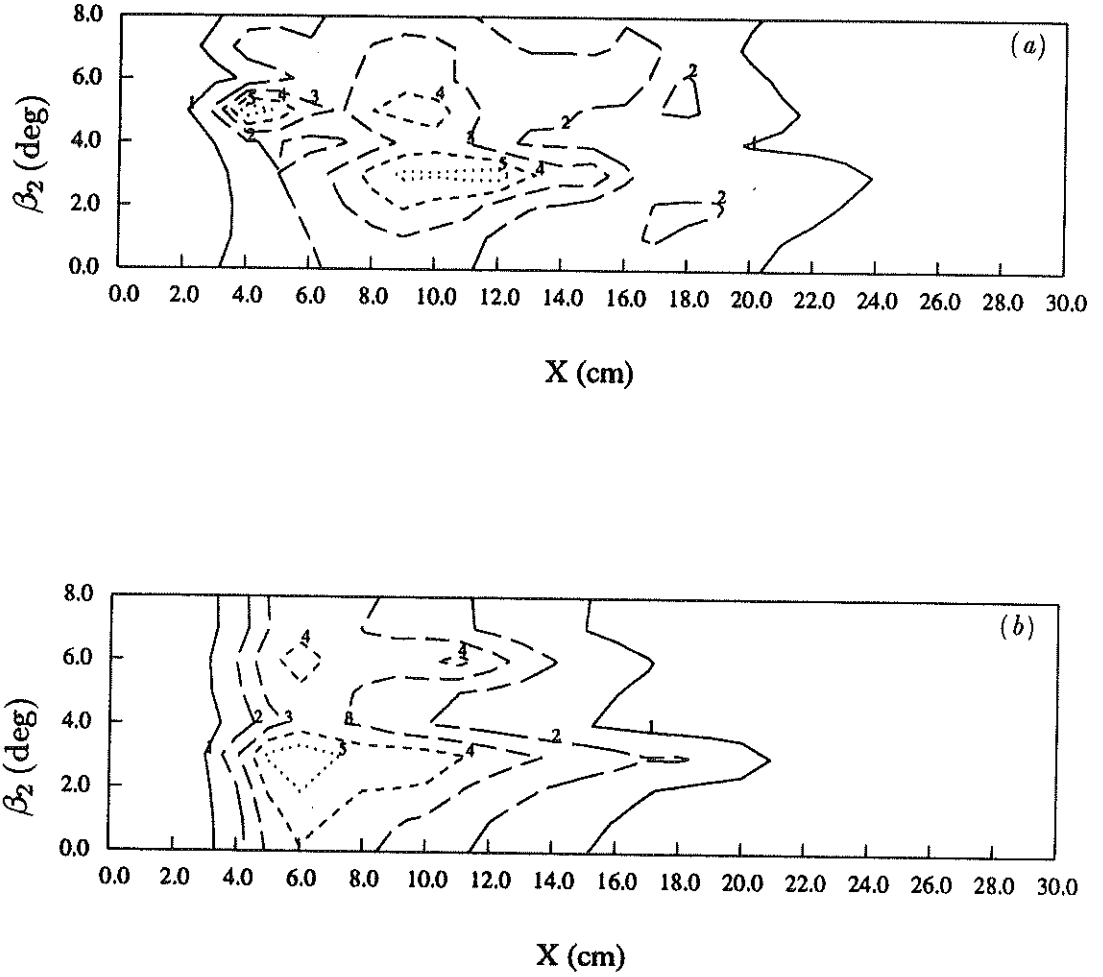

FIGURE 7. Streamwise development of fundamental centerline spectra. *(a)* u, levels are 0.001 ——— ; 0.004 — — ; 0.007 — — — ; 0.010 - - - - ; 0.013 ····· , *(b)* v, levels are 0.005 ——— ; 0.017 — — ; 0.029 — — — ; 0.041 - - - - ; 0.053 ····· , m^2.

streamwise TH grid spacing for the sampling rate used was then $\Delta\tilde{X} = 0.24$ cm (i.e. less than half the true grid spacing). A central difference scheme was used to calculate the spanwise vorticity which was then interpolated onto the true measurement grid. The spanwise vorticity generated using TH was then directly compared to that calculated from measured velocity components using a central difference scheme. Using the field shown in Fig. 3 as the reference (i.e. t = 0), the results of TH for locations before pairing ($X = 13$ cm), during pairing ($X = 20$ cm) and after pairing ($X = 25$ cm) are shown in Fig 9. The TH vorticity contours appear similar to their measured counterparts although a close examination reveals that they differ in shape and orientation.

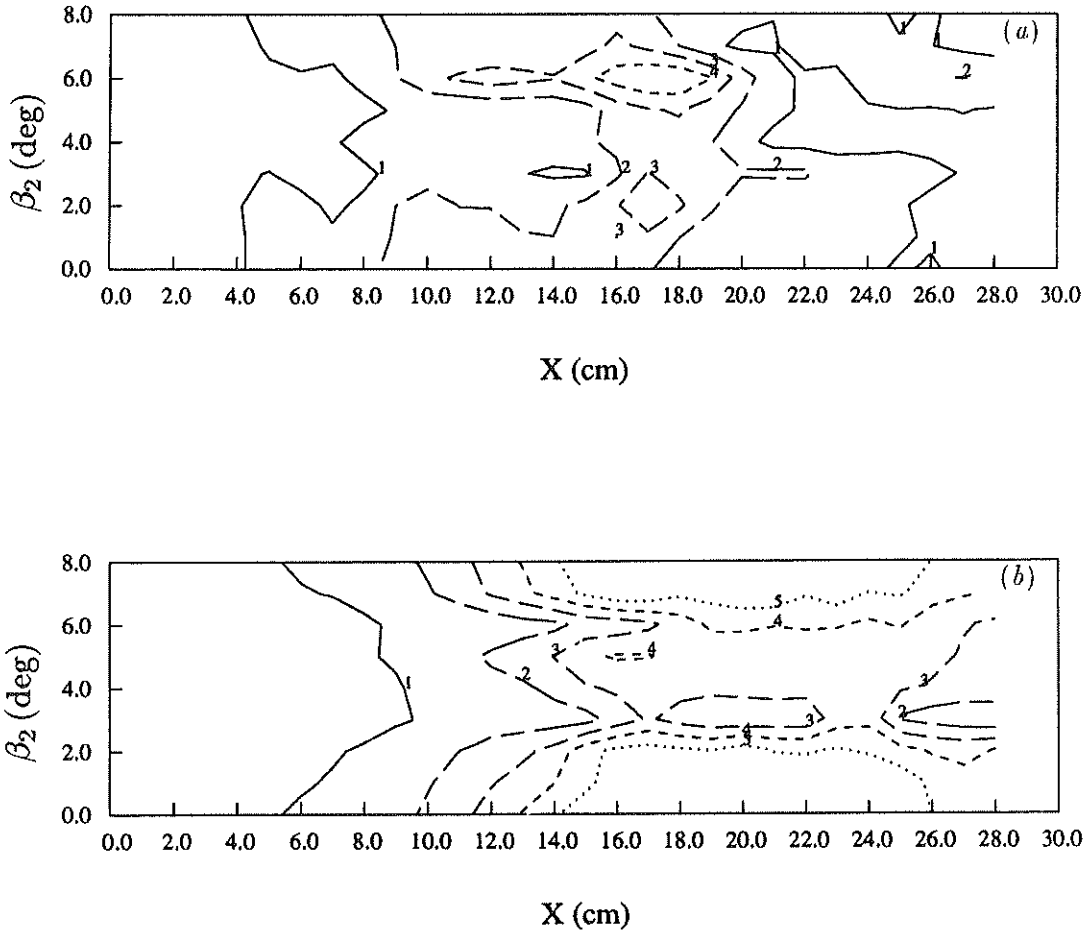

FIGURE 8. Streamwise development of subharmonic centerline spectra. *(a)* u, levels are 0.003 ——— ; 0.008— — ; 0.013— — — ; 0.018---- ; 0.023····· , m^2. *(b)* v, levels are 0.003——— ; 0.010— — ; 0.017— — — ; 0.024---- ; 0.031····· , m^2.

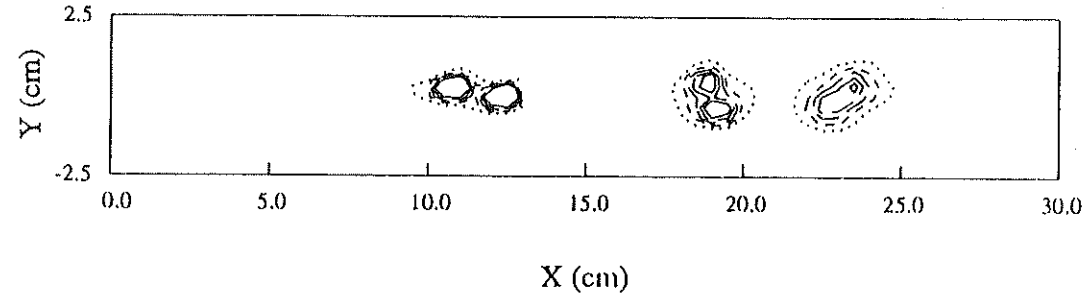

FIGURE 9. Centerplane spanwise vorticity calculated using Taylor's hypothesis at $X = 13$ cm, $X = 20.5$ cm and $X = 25$ cm normalized by $U_1 - U_2$ for $\beta_2 = 22.5°$, 0.125 ····· ; 0.25 ---- ; 0.375 ——— ; 0.5 — — ; 0.625 ——— (s^{-1}).

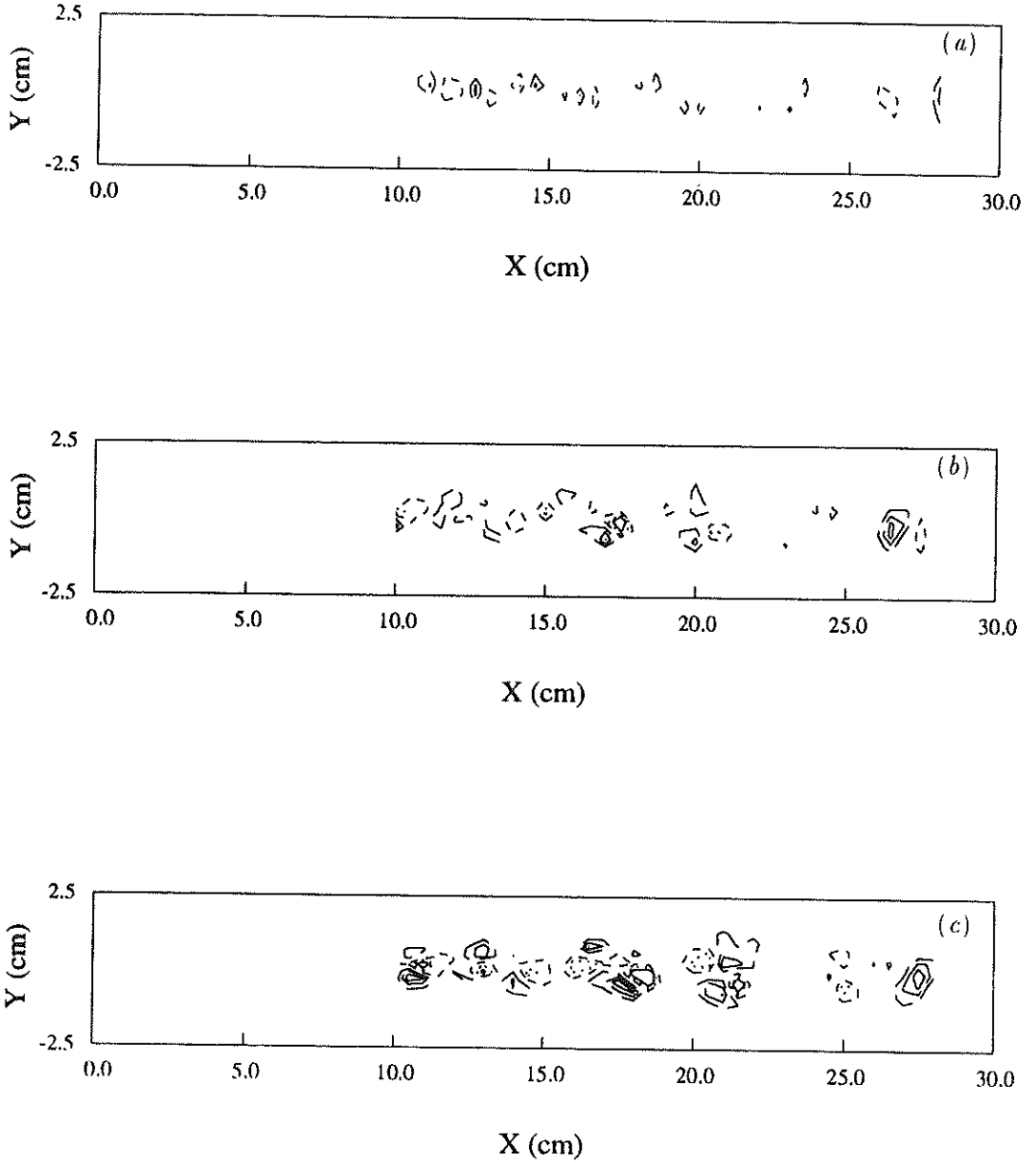

FIGURE 10. Centerplane spanwise vorticity error from using Taylor's hypothesis normalized by the peak spanwise vorticity. *(a)* $\Delta X = 0$ cm, *(b)* $\Delta X = 0$ cm, *(c)* $\Delta X = 0$ cm. -0.15 ——— (not in *(a)*); -0.10 — — ; -0.05 — — — ; 0.05 - - - - ; 0.10 ····· ; 0.15 —·— (not in *(a)*).

To quantify the error resulting from this approximation, the difference between true vorticity and the TH result, normalized by the peak true vorticity, is shown in Fig. 10. Each of these plots shows the error at a given distance from the measurement location (ΔX). The error for $\Delta X = 0$ is shown in Fig. 10 (*a*). The error would be expected to be zero since the measurement location and the approximation location coincide; however, the vorticity is calculated using differences of TH results offset from the true location. Of course, the errors resulting from using TH get progressively worse as the distance from the measurement location increases as shown in Figs. 10 (*b*) ($\Delta X = 1.0$ cm) and (*c*) ($\Delta X = 2.0$ cm). The failure of Taylor's hypothesis in this flow is especially prominent in the core of the spanwise vortices before, during, and after pairing. Since the peak vorticity is typically orders of magnitude greater than the vorticity of most of the field, the corresponding percent error of the approximated vorticity is in general several hundred percent for ΔX as low as 0.5 cm. These results confirm the observations of Zaman & Hussein (1981) that Taylor's Hypothesis should be avoided if the details of the mixing layer flow structure are of interest.

3. Future plans

During the remainder of the program, vortex interaction and transition to turbulence will be studied using benchmark three-dimensional phase-locked measurements of a plane mixing layer. In addition to the two pairing mechanisms observed in the two-dimensional data sets shown in this report (normal pairing and shredding), other combinations of forcing signals will be used to attempt to excite interactions such as tripling, the second pairing, and possibly the third pairing. In this manner, the pairing mechanisms which would normally occur randomly in time and space can be isolated and studied in a real flow. This systematic study of the mixing layer should not only increase the current level of understanding of mixing layer structure interactions, but also provide a valuable data base for computation validation.

Acknowledgements

This work is being performed in the Fluid Mechanics Laboratory, NASA Ames Research Center in collaboration with Dr. R. D. Mehta. We would like to thank Dr. J. H. Watmuff for many invaluable suggestions and helpful discussions of this work.

REFERENCES

BELL, J. H. & MEHTA, R. D. 1989 Design and Calibration of the Mixing Layer Wind Tunnel. *JIAA Report TR-84*. Dept. of Aeronautics and Astronautics, Stanford University.

BELL, J. H. AND MEHTA, R. D. 1992 Measurements of the Streamwise Vortical Structures in a Plane Mixing Layer. *J. Fluid Mech.* **239**, 213.

BERNAL, L. P. 1981 The Coherent Structure of Turbulent Mixing Layers I. Similarity of the Primary Vortex Structure. II. Secondary Streamwise Structure. *PhD thesis.* Calif. Inst. Tech.

BERNAL, L. P. & ROSHKO, A. 1986 Streamwise Vortex Structure in Plane Mixing Layers. *J. Fluid Mech.* **170,** 499-525.

BREIDENTHAL, R. 1981 Structure in Turbulent Mixing Layers and Wakes Using a Chemical Reaction. *J. Fluid Mech.* **109,** 1-24.

BUELL, J. C. 1991 A Hybrid Numerical Method for Three-Dimensional Spatially-Developing Free-Shear Flows. *J. Comp. Phys.* **95,** 313-338.

HUANG, L. S. & HO, C. M. 1990 Small-Scale Transition in a Plane Mixing Layer. *J. Fluid Mech.* **210,** 475-500.

INOUE, O. 1992 Double-Frequency Forcing on Spatially Growing Mixing Layers. *J. Fluid Mech.* **234,** 553-581.

MOSER, R. D. & ROGERS, M. M. 1993 The Three-Dimensional Evolution of a Plane Mixing Layer: Pairing and Transition to Turbulence. *J. Fluid Mech.* **247,** 275-320.

NYGAARD, K. J. & GLEZER, A. 1991 Evolution of Streamwise Vortices and Generation of Small-Scale Motion in a Plane Mixing Layer. *J. Fluid Mech.* **231,** 257-301.

RILEY, J. J. & METCALFE, R. W. 1980 Direct Numerical Simulation of a Perturbed Turbulent Mixing Layer. *AIAA Paper No. 80-0274.*

ROGERS, M. M. & MOSER, R. D. 1992 The Three-Dimensional Evolution of a Plane Mixing Layer: The Kelvin-Helmholtz Rollup. *J. Fluid Mech.* **243,** 183-226.

TUNG, C. H. 1992 Initial Streamwise Vorticity Formation in a Two-Stream Mixing Layer. *PhD Dissertation,* University of Houston.

WINANT, C. D. & BROWAND, F. K. 1974 Vortex Pairing: The Mechanism of Turbulent Mixing-Layer Growth at Moderate Reynolds Number. *J. Fluid Mech.* **63,** 237-255.

ZAMAN, K. B. M. Q. & HUSSEIN, A. K. M. F. 1981 Taylor Hypothesis and Large-Scale Coherent Structures. *J. Fluid Mech.* **112,** 379-396.

ZHANG, Y. Q. & HO, C. M. 1985 The Mixing Layer Forced by Fundamental and Subharmonic. In *IUTAM Symp. on Laminar-Turbulent Transition. Novosibirsk* (ed V. Kozlov), Springer, 385-395